

Atomic layer etching of high-k oxide thin films using hexafluoroacetylacetone and oxygen radicals

Jeongbin Lee¹, Jieun Oh¹, Jung-Tae Kim, Jiwoo Oh, Jeong-Min Lee¹, Woo-Hee Kim^{*}¹

Department of Materials Science and Chemical Engineering, BK21 FOUR ERICA-ACE Center, Hanyang University, Ansan, Gyeonggi 15588, Republic of Korea



ARTICLE INFO

Keywords:

Atomic layer etching
High-k oxides
4+ oxidation states
Hexafluoroacetylacetone
Etching mechanism

ABSTRACT

As integrated circuit devices continue to shrink, achieving sub-3 nm technology nodes requires innovative 3D architectures along with the advent of advanced materials and processes. From an etching perspective, traditional reactive ion etching (RIE), which uses reactive ions and neutral species, becomes increasingly inadequate for atomic-scale dimensions due to surface damage from ion bombardment and the high surface-to-volume ratio. Atomic layer etching (ALE) presents a superior alternative, utilizing two complementary self-limiting steps. By alternating between surface modification and removal phases, ALE enables atomic-level control over etching, surpassing the limitations of traditional RIE methods. In this study, we utilized hexafluoroacetylacetone (Hhfac) and O radicals, generated by a hollow cathode plasma source, as the primary etching agents for various high-k including HfO₂, ZrO₂, Al₂O₃, and Y₂O₃ thin films. Our research focused on elucidating the adsorption dynamics of Hhfac, which contribute to significant volatilization upon interaction with O radicals, leading to self-limiting etching with atomic-scale precision. Detailed surface reactions, mass variations, and volatile etch byproducts were systematically analyzed using X-ray photoelectron spectroscopy (XPS), *in-situ* quartz crystal microbalance (QCM), and *in-situ* residual gas analyzer (RGA). These analyses provided both theoretical and experimental insights into the etching mechanisms. This work presents a layer-by-layer removal method for various high-k materials, enabling the creation of sharp interfaces and high aspect ratio patterns and contributes to a deeper understanding of etching pathways, particularly in the Ångström era of device scaling.

1. Introduction

As the dimensions of complementary metal–oxide–semiconductor (CMOS) devices continue to shrink with advances in electronic manufacturing, it is expected that the technology node for modern logic devices will scale down to below 3 nm, enabling higher performance and increased transistor density [1]. This ongoing reduction in device dimensions has necessitated the adoption of new materials and processes compatible with advanced 3D nanodevice integration, such as gate-all-around (GAA) transistors, which feature high surface-to-volume ratios [2–4]. Particularly, atomic layer deposition (ALD) of high-k oxides such as HfO₂, ZrO₂, and Al₂O₃, with their high dielectric constants (k), low electrical leakage, and excellent thermal stability, has been widely utilized as replacements for SiO₂ in modern semiconductor devices for over 10 years [5]. More recently, there has been a need to precisely reduce the thickness of high-k oxides while preserving the crystallinity that emerges beyond a certain thickness, driven by performance and

geometric limitations. Additionally, achieving precise etching profiles of high-k oxides without footing issues has led to their consideration as potential hard mask materials in next-generation EUV lithography, enabling accurate pattern transfer with vertical sidewalls [6].

In this context, precise etching techniques are essential to remove such high-k materials with atomic-scale fidelity while avoiding over-etching and preventing damage to underlying substrates, crucial for meeting the stringent demands of device performance in complex 3D semiconductor architectures [7–9]. Traditional reactive ion etching (RIE), which relies on the exposure of chemically reactive ions and neutral species, has long been the foundational etching technology [10,11]. However, as the critical dimensions and profiles approach atomic-scale levels, particularly within extremely downscaled 3D structures, such conventional RIE method has become increasingly inadequate for satisfying the demanding requirements of plasma etching [12]. Furthermore, miniaturized and thinner device structures are highly vulnerable to surface damage from ion bombardment during

* Corresponding author.

E-mail address: wooheekim@hanyang.ac.kr (W.-H. Kim).

¹ These authors (J. Lee and J. Oh) contributed equally to this work.

plasma etching, which can lead to performance degradation, increased variability, and reduced reliability [12].

Accordingly, compared to the RIE process, atomic layer etching (ALE) has emerged as a self-limited technique designed to achieve monolayer-level precision in material removal [12,13]. Each ALE cycle consists of two distinct reactions. The first reaction, known as the surface modification step, involves the interaction of incoming chemical species, such as precursors or activated radicals, with the underlying substrate, resulting in the formation of a chemically modified layer [10]. This modified layer reduces the threshold energy required for its removal and prevents unintended etching of the underlying material. The second reaction involves ion bombardment, where moderate-energy ions provide sufficient kinetic energy to selectively remove the chemically modified layer [10,13]. This removal step ensures precise elimination of the modified layer while protecting non-targeted areas, enabling outstanding etch selectivity, layer-by-layer etching, and minimal damage to the material beneath.

In the first step of chemical modification, thermal adsorption can be utilized in lieu of plasma modification, enabling the formation of a modified layer with greater atomic-scale fidelity. This method offers a more precise and controlled modification compared to plasma-based techniques, ensuring better consistency and minimizing damage to the underlying material. This thermal adsorption method is particularly advantageous when combined with diketones, which have been studied as one of effective precursors for ALE of metal or metal oxide films due to their exceptional reactivity and strong affinity for metals [14–17]. These diketones feature two oxygen atoms capable of simultaneously binding to a single metal center, forming stable chelate complexes. The tunable nature of diketones allows for modifications to the ligand groups, impacting steric effects, acidity, and volatility, thereby enabling tailored etch rates and selectivity [17]. When used in ALE of metal or metal oxides with diketonates, the ALE process typically begins with an oxidation or chlorination step to elevate the metal to a higher oxidation state. This is followed by the chelation step, where diketones, such as hexafluoroacetylacetone (Hhfac) and acetylacetone (Hacac), form volatile metal-ligand complexes [15–19]. However, while diketones are well-known for their remarkable coordination capabilities, their use in ALE for metal oxides has been primarily limited to those with +2 oxidation states, such as ZnO and CoO. This limitation arises from the steric hindrance associated with higher oxidation states, which complicates the formation of stable, volatile chelate complexes. Specifically, the requirement for three or four acac or hfac ligands to induce volatility is hindered by spatial constraints, making it difficult to form stable complexes with high-valency metals. As a result, no prior studies have specifically explored ALE for high-k thin films such as HfO₂ and ZrO₂, which exhibit 4+ oxidation states (i.e., Hf⁴⁺, Zr⁴⁺) and present additional challenges in forming volatile complexes. Indeed, previous ALE studies on ZnO films using Hacac and O₂ plasma demonstrated exceptional selectivity against Al₂O₃ (~8:1) and SiO₂/HfO₂ (~80:1), highlighting the inefficiency of diketone-based volatilization for these oxides [17]. Furthermore, a comprehensive understanding of the exact etch by-products and underlying etching mechanisms remains yet to be explored. Furthermore, although several attempts have been made to utilize theoretical calculations and modeling to elucidate reaction mechanisms at the atomic-scale processing, [20–22] a comprehensive understanding of the exact etch by-products and underlying etching mechanisms remains yet to be explored.

In this study, therefore, we introduce the use of Hhfac molecules as a diketonate precursor to chemically induce the formation of a surface-modified layer on various high-k dielectric materials, including HfO₂, ZrO₂, Al₂O₃ and Y₂O₃ films. To optimize the volatilization of the modified layer in the subsequent step of the ALE process, we employed a remote hollow cathode plasma (HCP) source, which generates neutral oxygen radicals. Compared to direct capacitively coupled plasma (CCP) sources, this remote plasma configuration provides higher radical densities while minimizing plasma-induced damage to the substrate. This

study systematically investigates the ALE characteristics and fundamental aspects of the proposed ALE chemistry, primarily focusing on the temperature-dependent adsorption dynamics of Hhfac molecules, which pertain to their crucial role in volatilization upon exposure to subsequent O radicals, especially for high-k oxides with 4+ oxidation states. To uncover the detailed molecular interactions and mechanistic pathways, a combination of techniques was employed, including X-ray photoelectron spectroscopy (XPS) for surface composition analysis, *in-situ* quartz crystal microbalance (QCM) for real-time mass variation monitoring, and residual gas analysis (RGA) for identifying volatile etch byproducts. By advancing our understanding of the ALE mechanism for high-k materials, these findings pave the way for the practical integration of ALE into semiconductor manufacturing, enabling precise etching of high-k oxide films such as HfO₂ and ZrO₂.

2. Experimental details

2.1. ALE process

In this study, the ALE process was performed using a 4-inch traveling-wave type ALE reactor (Atomic Classic, CN-1 Co.) equipped with a hollow cathode plasma (HCP) system (Series 50, Meaglow Ltd.). The HCP source, operating at a 13.56 MHz radio frequency (RF), was positioned approximately 10 cm above the substrate. One ALE cycle consists of sequential exposure of 1,1,1,5,5-hexafluoro-2,4-pentanedione (Hhfac) (98+, Alfa Aesar) precursor and oxygen radicals. The Hhfac precursor was stored in a room-temperature stainless steel canister and delivered at 0.3 Torr via a metering valve. To remove any excess molecules and etching by-products, a 30-second purge with high-purity N₂ (99.999%) was carried out between each pulse. A parallel plate capacitively coupled plasma (CCP) reactor (Nexusbe Co., Ltd.) was employed to evaluate etching performance.

2.2. Substrate preparation

For the ALE experiments, HfO₂, ZrO₂, Y₂O₃ and Al₂O₃ thin films deposited by ALD methods on a Si substrate. HfO₂, ZrO₂ and Y₂O₃ ALD processes were conducted at a deposition temperature of 320 °C using cyclopentadienyl tris(dimethylamino)hafnium [CpHf(NMe₂)₃] (iChems Co., Ltd.), cyclopentadienyl tris(dimethylamino)zirconium [CpZr(NMe₂)₃] (iChems Co., Ltd.), and (RCp)₂Y(iPr-amd) (IYA02, iChems Co.), respectively, with ozone (O₃, 220 g/m³) as the co-reactant. The Al₂O₃ ALD process involved the use of trimethylaluminum [Al(CH₃)₃] (iChems Co., Ltd.) as the precursor, with H₂O as the co-reactant at 150 °C. Si substrates, 23 nm thick SiO₂ grown thermally, and 32 nm thick SiN fabricated using plasma-enhanced chemical vapor deposition (PECVD) were separately prepared as references for etching.

2.3. Analytical methods

The etched thickness of the films was characterized using a spectroscopic ellipsometer (MG-1000, Nano View Co.) with a spectral range of 380–900 nm at a 70° fixed incidence light angle. The layer density of the films was estimated by energy-dispersive X-ray fluorescence (EDXRF) (ARL Quant'X, Thermo Fisher Scientific Co.). The film surface morphology was analyzed using an atomic force microscope (AFM) (Park XE-100) with a scan size of 5 × 5 μm², and the root mean square (RMS) surface roughness values were extracted from the standard deviation of the height values in the AFM images. The elemental composition and chemical binding structures of various surfaces were analyzed by angle-resolved X-ray photoelectron spectroscopy (AR-XPS) (K-alpha plus, Thermo Fisher Scientific Co.) with an Al Kα X-ray source of 1486.6 eV, using the C 1 s (C-C bonding, 284.5 eV) peak as a reference to calibrate the measured core levels. The built-in quartz crystal microbalance (QCM) (SQM-160, Inficon) with a 6 MHz quartz crystal (285 °C optimized crystals, 14 mm gold), positioned at a typical substrate

location and at almost the same azimuthal angle as that of the substrate, was used to determine the mass change per cycle during the ALE process. To identify a plausible etching reaction mechanism, *in-situ* mass spectrometry measurements were conducted using a residual gas analyzer (RGA-200, Stanford Research Systems) in the range of 1 to 200 amu with a mass resolution of 1 amu. The ionization energy of the RGA was fixed at 70 eV. Prior to etch measurements, the RGA was calibrated using Ar, CO, CO₂, H₂, and H₂O to ensure accurate quantification of gas components.

3. Results and discussion

Fig. 1a illustrates the four principal repetitive steps of the ALE process: the Hhfac-induced surface modification step and the O radical-induced removal step via oxidative bond cleavage, separated by N₂ purging steps that effectively remove undesired etching residues and prevent cross-contamination. **Fig. 1b** schematically illustrates the overall etching mechanism. Initially, Hhfac molecules adsorb onto the high-k oxide surface, where dissociative chemisorption results in the formation of fluorinated surface species such as CF_x and OC_x. These species chemically passivate and modify the topmost layer, thereby lowering its binding energy. In the subsequent step, oxygen radicals generated from the HCP source react with the modified surface. These radicals induce a series of oxidation reactions that cleave molecular bonds, forming volatile compounds such as Hf-CF_x and Hf-OC_x. This process enables chemical fragmentation and volatilization of surface species, rather than physical desorption of intact layers. The layer-by-layer removal is corroborated by *in-situ* QCM measurements of mass variation and RGA analysis of volatile byproducts.

As depicted in **Fig. 2a**, the ALE process was conducted for 100 cycles, with each cycle consisting of a 5 s Hhfac pulse, a 30 s N₂ purge, a 15 s O radical pulse, and another 30 s N₂ purge, applied under a 200 W bias power. Substrate temperatures ranging from 100 to 400 °C were used to evaluate the etch per cycle (EPC) of HfO₂, ZrO₂, Al₂O₃, Y₂O₃, Si, SiO₂, and SiN films. The EPC values for HfO₂ (black circles in **Fig. 2**) were estimated to be 0.01 ± 0.01, 0.03 ± 0.01, 0.12 ± 0.07, 0.24 ± 0.06, 0.59 ± 0.11, 0.67 ± 0.08, and 0.81 ± 0.16 Å/cycle at substrate temperatures of 100, 150, 200, 250, 300, 350, and 400 °C, respectively. Similarly, ZrO₂ (red circles in **Fig. 2**) exhibited EPC values of 0.04 ± 0.02, 0.08 ± 0.02, 0.25 ± 0.06, 0.66 ± 0.10, 0.84 ± 0.09, 0.93 ± 0.09, and 1.33 ± 0.12 Å/cycle over the same temperature range. Under identical temperature conditions, Al₂O₃ (blue circles in **Fig. 2**) showed EPC values of 0.04 ± 0.01, 0.06 ± 0.04, 0.21 ± 0.08, 0.35 ± 0.05, 0.69

± 0.07, 0.82 ± 0.13, and 1.20 ± 0.20 Å/cycle. The EPC values for Y₂O₃ increased steadily from 0.21 ± 0.05 Å/cycle at 350 °C to 0.93 ± 0.20 Å/cycle at 400 °C, while SiO₂ and SiN films exhibited almost negligible etching behavior (see Fig. S1 in Supplementary Information). These temperature-dependent etching behaviors are summarized in Table S1, which presents the detailed EPC values for HfO₂, ZrO₂, Al₂O₃, and Y₂O₃ across the temperature range of 100–400 °C under a constant RF bias power of 200 W. The prominent increase in EPC with rising substrate temperature can be attributed to the thermally activated nature of the modification and desorption reactions.

Fig. 2b-d illustrate the EPCs for HfO₂, ZrO₂, and Al₂O₃, which were obtained by varying the bias power and injection time of the etchant sources over 100 ALE cycles at 300 °C. **Fig. 2b** shows that ALE is highly dependent on the energy and flux of O radicals, which can be controlled through substrate biasing. At bias power below 150 W, referred to as the incomplete etch regime, the EPC for all samples increased with increasing bias power. Once the bias power exceeded 150 W within the ALE window, O radicals above the desorption threshold facilitated the complete removal of the modified layer. The physical sputtering region, including Y₂O₃, Si, SiO₂, and SiN films, was not observed up to a bias power of 500 W, as reported in Fig. S1. Table S2 summarizes the detailed EPC values for the same oxide materials as a function of RF bias power (0–300 W) at a fixed temperature of 300 °C, providing insight into RF power-dependent etch characteristics. The saturated EPC values were found to be 0.57 Å/cycle for HfO₂, 0.85 Å/cycle for ZrO₂, and 0.68 Å/cycle for Al₂O₃, with respective Hhfac and O radical feeding times of 1 s/8 s, 1 s/7 s, and 1 s/6 s, demonstrating the self-limiting nature of the ALE process, as shown in **Fig. 2c** and **2d**. The EPC values measured by EDXRF were 0.058 µg/(cm²·cycle) for HfO₂ and 0.044 µg/(cm²·cycle) for ZrO₂ over 300 ALE cycles, as detailed in Fig. S2. The AFM-derived RMS surface roughness images and line scans of the HfO₂ film before and after etching are shown in Fig. S3. During 50 cycles of ALE, which removed 2.76 nm of HfO₂, the RMS roughness decreased from 0.634 nm to 0.547 nm, resulting in a smoother surface.

Fig. 3a demonstrates the examination of the synergistic etching mechanism for Hhfac and oxygen sources through three approaches: Hhfac-only dosing, cyclic dosing of Hhfac with O₂ gas, and cyclic dosing of Hhfac with O radicals, each yielding distinct trends in film thickness evolution. Mohimi *et al.* previously reported that copper oxide reacts with Hhfac to yield volatile Cu(hfac)₂;[16] however, in our results, merely injecting Hhfac on all samples did not result in any thickness changes. This observation confirms the fundamentally different surface

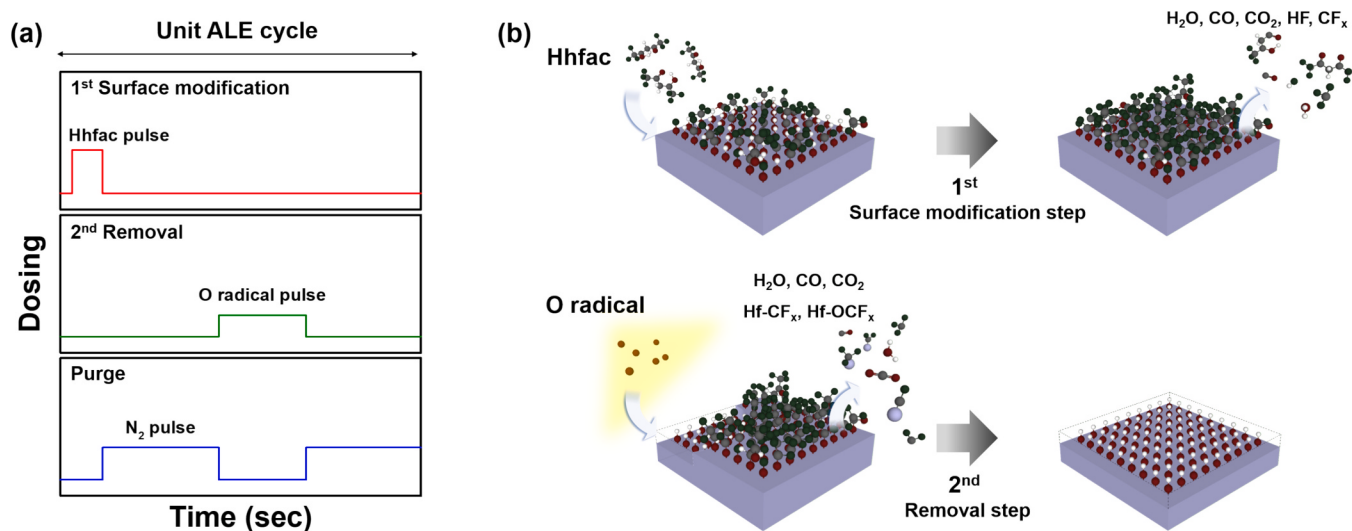


Fig. 1. Schematic of (a) the unit ALE sequence and (b) the layer-by-layer etch mechanism, illustrating how the initial exposure to Hhfac facilitates surface modification, while subsequent O radicals enable self-limiting removal of the modified region.

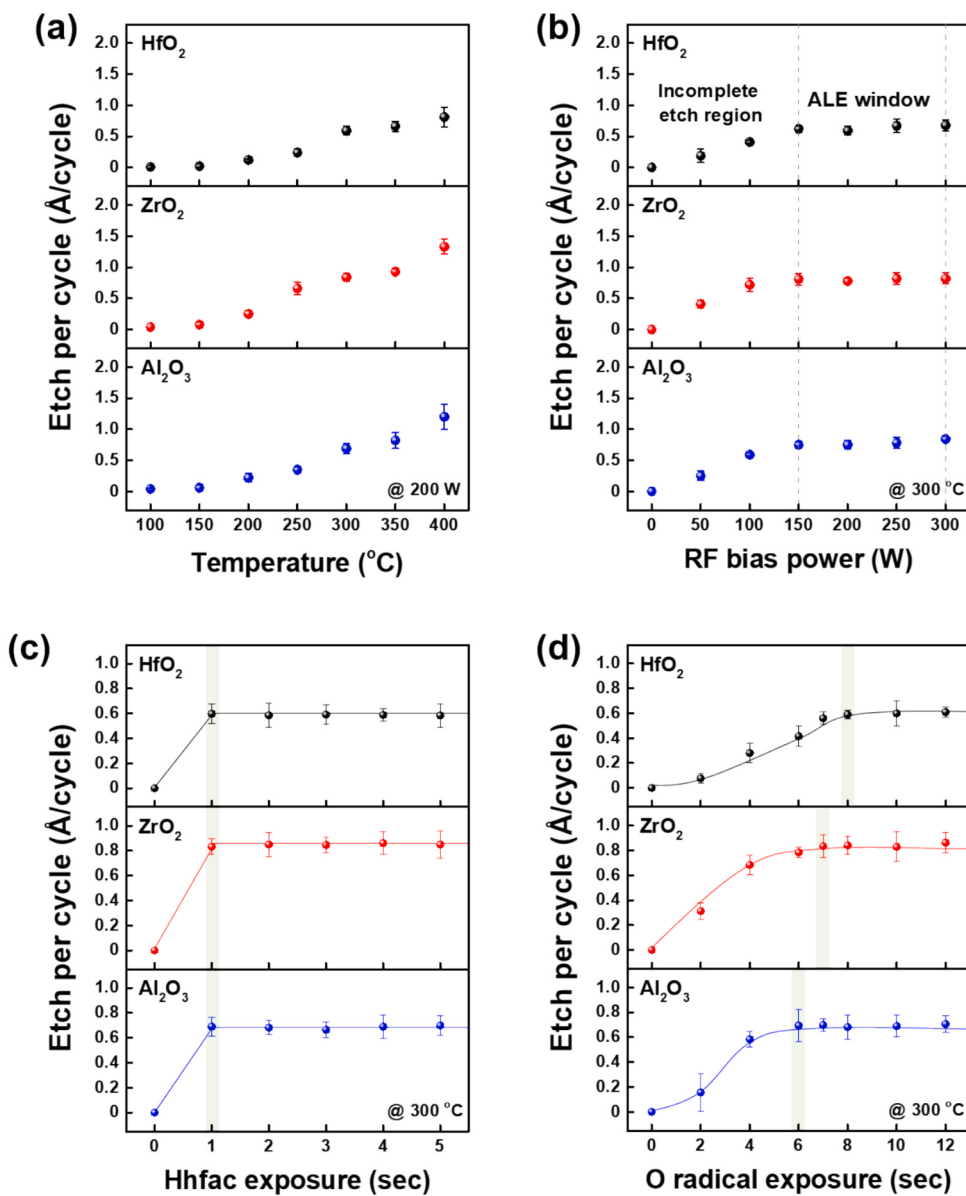


Fig. 2. Etch rates for HfO₂, ZrO₂, and Al₂O₃ films with respect to (a) substrate temperature, (b) RF bias power, (c) Hhfac pulse time, and (d) O radical pulse time.

reactivity of HfO₂ and ZrO₂ compared to CuO, as their highly coordinated, dense oxide lattices restrict access of bulky Hhfac ligands to the metal centers, thereby rendering the cooperative coordination required for highly volatile metal-hfac complexes, such as Hf(hfac)₄ and Zr(hfac)₄, both sterically hindered and thermodynamically unfavorable [23–25]. Moreover, film thicknesses remained constant under consecutive pulses of Hhfac and O₂ gas, establishing that O₂ gas alone is insufficient to remove the Hhfac-modified surface layer. Remarkably, the consistent thickness decrease observed when Hhfac and O radicals are sequentially combined highlights that radical-driven chemical removal is essentially required for an effective ALE process.

In-situ QCM experiments were conducted to further investigate the synergistic etching effect by successively dosing Hhfac with O₂ gas or O radicals. Fig. 3b illustrates the mass change per cycle for real-time QCM measurements during 12 cycles of repeated Hhfac and O₂ gas dosing, followed by 40 ALE cycles on HfO₂ at a substrate temperature of 300 °C. The first 12 cycles using O₂ gas showed no significant mass loss, which is consistent with the results shown in Fig. 3a. For the following 40 cycles of Hhfac and O radical dosing, a mass gain of approximately 10 ng/cm² per cycle was observed after Hhfac dosing, attributed to the passivation

effect from the adsorption of Hhfac molecules onto the surface. Following the O radical pulse, a cumulative mass loss of about 60 ng/cm² per cycle was observed, corresponding to the radical-driven removal of the modified HfO₂ layer. The QCM measurements revealed a mass gain of only ~ 10 ng/cm² per Hhfac pulse, quantitatively confirming the steric hindrance phenomenon hypothesized in our etching mechanism and demonstrating restricted surface coverage of Hhfac ligands. Based on its molecular weight (~616 g/mol) and crystallographic footprint (100–130 Å² per molecule) [23], a densely packed monolayer would correspond to approximately 80–100 ng/cm². This notable discrepancy is primarily attributed to dissociative adsorption at 300 °C, where Hhfac molecules decompose upon surface contact rather than adsorbing intact. Although steric hindrance around Hf(IV) centers limits molecular adsorption, the dominant factor is temperature-driven dissociation, resulting in a surface terminated by smaller CF_x and OCF_x fragments. This analysis supports our overall etch mechanism, which proposes a transition from molecular to dissociative adsorption as a function of temperature, essential for achieving effective etching during subsequent O radical exposure.

Next, the surface modification of HfO₂ was examined using AR-XPS

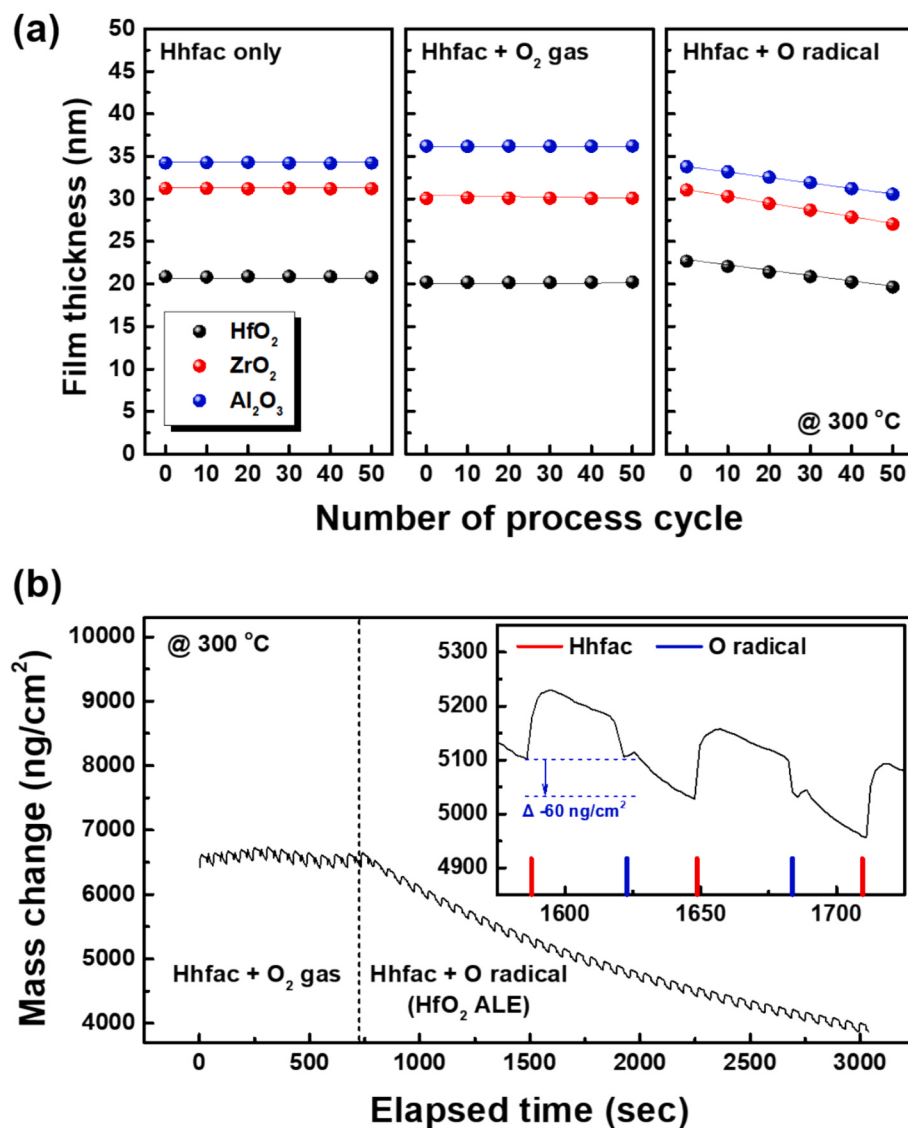


Fig. 3. (a) The progression in thickness as a function of the number of pulses or cycles for Hhfac-only pulses, consecutive Hhfac and O₂ gas pulses, and ALE cycles incorporating both Hhfac and O radical pulses. (b) Real-time QCM measurements during 12 cycles of repeated Hhfac and O₂ gas dosing, followed by 40 ALE cycles on HfO₂ at a substrate temperature of 300 °C. The inset shows the magnified region from 1600 to 1700 s.

measurements before and after 60 s of Hhfac exposure at 100 °C and 300 °C, following 60 s of O radical pre-clean. Fig. 4a-d present high-resolution Hf 4f, O 1 s, C 1 s, and F 1 s spectra acquired at an emission angle of 80° with respect to the sample normal. Fig. 4a shows the deconvolution of the Hf 4f spectrum, revealing two peaks corresponding to Hf 4f_{7/2} and Hf 4f_{5/2}, located at 16.8 eV and 18.4 eV, respectively, which are characteristic of Hf–O bonds [26]. Compared to pure HfO₂, the Hhfac-treated samples exhibit an increase in binding energy of approximately 0.1 eV for both the Hf 4f_{7/2} and Hf 4f_{5/2} peaks. This shift might be associated with the formation of a modified fluorocarbon layer on the HfO₂ surface or the partial passivation of oxygen vacancies by incorporated fluorine atoms [27]. The O 1 s core-level spectrum in Fig. 4b was deconvoluted into three peaks at 530.2 eV, 532.1 eV, and 532.0 eV, corresponding to lattice oxygen (Hf–O bonding), non-lattice oxygen (O–O bonding), and a combination of ester or carboxylic and fluorinated carbonyl groups (O–C, O=C, and O–CF_x bonding), respectively [28,29]. Upon exposure to Hhfac molecules at 300 °C, the proportion of fluorinated carbonyl bonds increased to 26.22%, attributed to the surface adsorption of hfac ligands (*i.e.*, associative adsorption in monodentate, bidentate, and chelate forms, as illustrated in Fig. S4 in the Supporting Information) [30].

Unlike the Hf 4f and O 1 s spectra, which exhibited no significant changes in peak positions or intensities after Hhfac exposure, the C 1 s and F 1 s spectra showed distinct spectral variations, reflecting the formation of fluorinated carbon species. The C 1 s spectrum was deconvoluted into five distinct peaks: 284.5 eV, assigned to aliphatic carbon (C–C) [31]; 287.8 eV, corresponding to C–O, C=O, and O–CF_x bonds [32]; 88.7 eV, attributed to the –CF bond [33]; 291.0 eV, associated with the –CF₂ bond [34]; and 295.0 eV, assigned to the –CF₃ bond, as displayed in Fig. 4c [35]. Similarly, the F 1 s spectrum in Fig. 4d exhibited five deconvoluted peaks: Hf–OF_x at 685.5 eV, –CF at 688.5 eV, –CF₂ at 689.0 eV, and –CF₃ at 691.0 eV [36–38]. In comparison with the C 1 s and F 1 s spectra at 100 °C, the emergence of several CF_x-related surface moieties at 300 °C, suggests that thermal modification at the elevated temperature facilitates the dissociative adsorption of Hhfac molecules [39]. This dissociative adsorption leads to the formation of volatile etching products upon exposure to subsequent oxygen radicals, rather than being removed through the formation of volatile Hf(hfac)₄ complexes.

Fig. 4e presents the relative atomic percentages for various HfO₂ samples which was initially pre-cleaned with a 60 s O radical treatment,

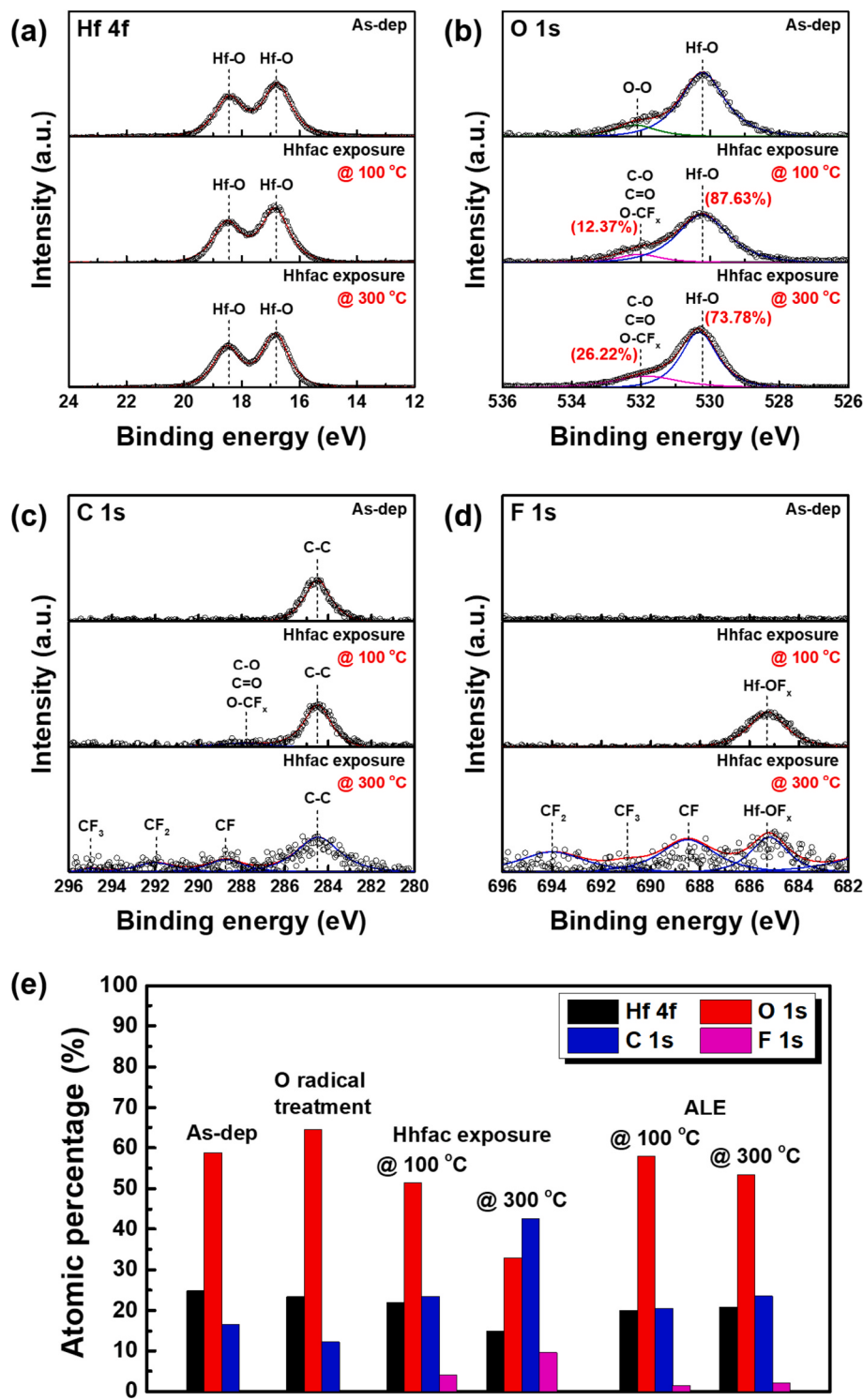


Fig. 4. AR-XPS analysis of as-deposited HfO_2 and HfO_2 treated with Hhfac at 100 °C and 300 °C, focusing on (a) Hf 4f, (b) O 1s, (c) C 1s, and (d) F 1s spectra. (e) XPS atomic composition of as-deposited HfO_2 , HfO_2 after O radical treatment, HfO_2 after Hhfac exposure at 100 °C and 300 °C, and HfO_2 following 30 ALE cycles at the same temperatures. The atomic composition for HfO_2 after Hhfac exposure was obtained from the XPS spectra in (a)–(d), while the data for 30 ALE cycles was obtained from Fig. S5.

followed by either 60 s of Hhfac exposure or 30 cycles of ALE at 100 °C and 300 °C, respectively. The atomic composition after 60 s of Hhfac exposure was obtained from the XPS spectra of the same samples shown in Fig. 4a–d, while the data for 30 cycles of ALE was derived from the XPS spectra in Fig. S5. For all samples, the atomic C content remains above 10% due to adventitious C contamination from the *ex-situ* nature of the XPS measurement. Upon exposure to Hhfac at 100 °C, the atomic

composition reveals that C constitutes 23.4% and F accounts for 4.1%, primarily attributed to the molecular adsorption of Hhfac without significant decomposition. As the temperature increases, the thermal decomposition of Hhfac may lead to a relatively higher accumulation of residual C and F species on the surface, reaching atomic percentages of 42.6% and 9.6%, respectively, at 300 °C. For the ALE samples at 100 °C, no significant difference in the residual C and F contents was observed

compared to the Hhfac exposure-only samples. This might be attributed to the minimal etching observed in Fig. 2a, suggesting that at low temperatures, only limited chemisorption of Hhfac molecules occurs. Alternatively, the incorporation of persistent C and F species likely results from the continuous ALE process. In contrast, for the ALE samples at 300 °C, a substantial reduction in C and F contents was observed compared to the Hhfac exposure-only samples. This reduction is likely due to the efficient dissociative adsorption of Hhfac molecules at the higher temperature, coupled with the formation of volatile etching byproducts through interaction with O radicals. Nevertheless, the presence of persistent C and F components at levels similar to those observed at 100 °C was still detected.

To investigate the dissociated ion species during each temporal reaction, *in-situ* residual gas analyzer (RGA) measurements were utilized, as shown in Fig. 5. The RGA cracking patterns of Hhfac exposure at stage temperatures between 100 °C and 300 °C are displayed in Fig. 5a, showing mass-to-charge ratios (m/z) from 1 to 100 amu, while Fig. 5b focuses on the 100 to 200 m/z range. Notable signals were detected at 20, 28, 31, 47, 50, 69, 119, and 139 m/z , corresponding to HF^+ , CO^+ , CF^+ , OCF^+ , CF_2^+ , CF_3^+ , $[\text{hfac-CF}_3\text{-HF}]^+$, and $[\text{hfac-CF}_3]^+$, respectively. The formation of HF^+ and $[\text{hfac-CF}_3\text{-HF}]^+$ is proposed to arise from intramolecular hydrogen bonding interactions between O-H and F-C groups, which act to stabilize the intermediates during the reaction [40]. CF^+ and CF_2^+ species are presumed to result from the homolytic cleavage of CF_3 as fluorine atoms are transferred to the substrate.

With increasing stage temperatures, the ion intensities for CF^+ , CF_2^+ , and CF_3^+ peaks increase, as also observed in Fig. S6, whereas the signals for $[\text{hfac-CF}_3\text{-HF}]^+$ and $[\text{hfac-CF}_3]^+$ progressively diminish and eventually vanish due to the heat-induced decomposition of Hhfac. Annealing to temperatures exceeding 300 °C causes the Hhfac moiety to completely decompose, leaving surface-bound species containing fluoroalkyl ether groups, which contribute to the etching process. The proposed mechanism likely involves the chemisorption and partial decomposition of Hhfac molecules on the oxide surface, leading to the incorporation of ligand-derived fluorine into the outermost layer [41]. This fluorinated surface layer represents an essential intermediate phase in the etching sequence. Subsequent exposure to oxidative species initiates the breakdown of this modified layer, facilitating material removal in a controlled and self-limiting manner.

Fig. 5c and 5d depict the RGA mass spectrum and the time-resolved ion intensity profiles showing etch products recorded over 60 s of O radical interaction with Hhfac-coated HfO_2 at 300 °C, respectively. After 500 cycles of ALD HfO_2 , the Hhfac exposure was maintained for 10 min at 300 °C to enhance adsorption efficiency and strengthen RGA signal amplitude. The absence of signals aside from O^+ and O_2^+ ions during O_2 gas utilization implies that O_2 gas lacks the capability to energetically remove the polymerized layer on the material surface. On the other hand, the significant m/z at 18, 20, 28, 31, 44, and 47 are assigned to H_2O^+ , HF^+ , CO^+ , CF^+ , CO_2^+ , and OCF^+ , respectively. Considering these main ion signals and Langmuir–Hinshelwood kinetics, the addition of

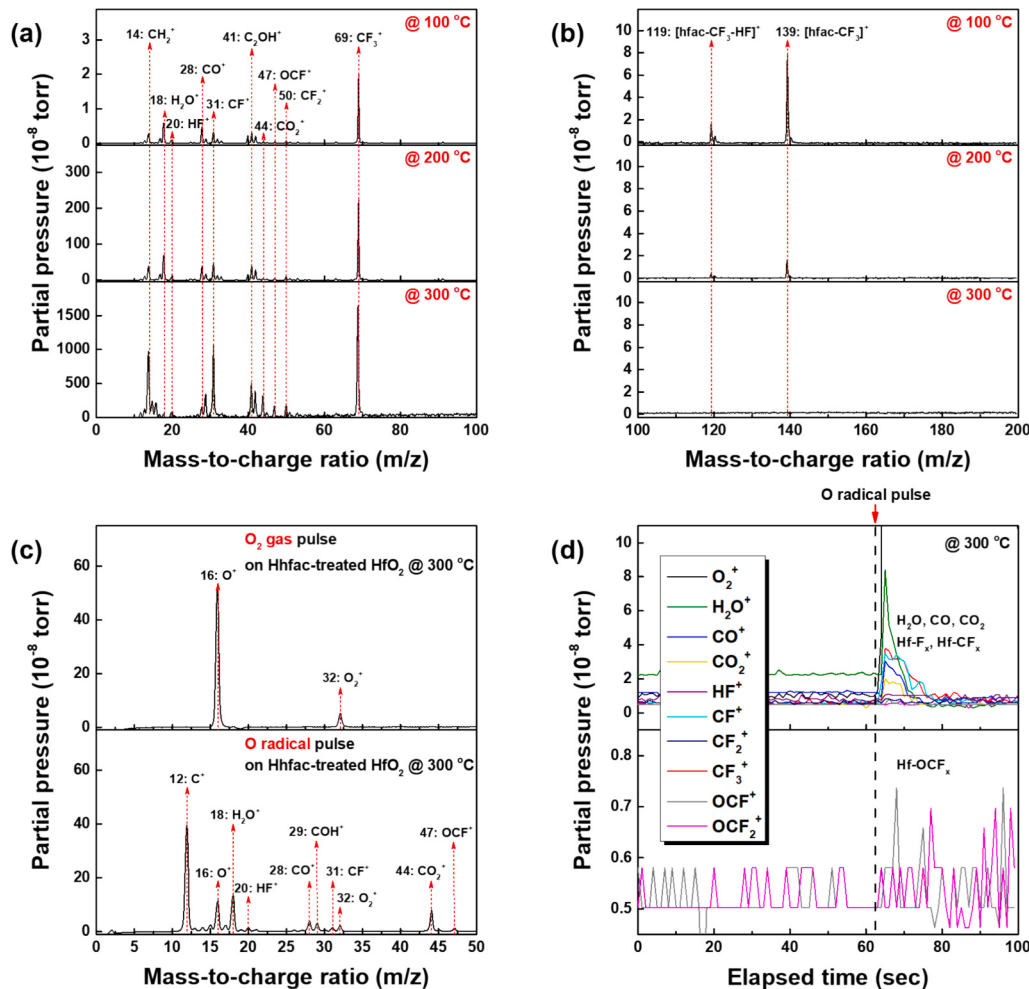


Fig. 5. RGA mass spectra displaying mass-to-charge (m/z) ranges of (a) 1–100 atomic mass units (amu) and (b) 100–200 amu. (c) Ion products identified in the RGA mass spectra after exposing Hhfac-covered HfO_2 to O_2 gas and radicals. (d) Time-resolved ion intensity profiles of etch species during a 60-second O radical exposure on Hhfac-covered HfO_2 at 300 °C.

oxygen radicals leads to the formation of volatile byproducts, including Hf-F_x, Hf-CF_x, Hf-OCF_x, CO, CO₂, and H₂O, through chemical sputtering between oxygen radicals and the less-volatile modified layer [42]. Fluorocarbonated surfaces serve as active sites for this radical-stimulated combustion reaction. The RGA used in this study, with a measurable range limited to 1–200 amu, cannot directly identify high-mass Hf-mediated fluoroalkyl compounds; for instance, Hf-CF, Hf-OCF₂, and Hf-CF₃, which have *m/z* values around 209, 244, and 247, respectively. Therefore, these compounds are instead tracked indirectly via CF_x or OCF_x fragments. The systematic increase in these fragment intensities (*m/z* 20, 28, 31, 44, and 47) specifically observed during O radical injection supports the formation of volatile Hf-containing etch byproducts during the ALE process.

To further elucidate the proposed etching mechanism, we performed an ALE process using a CCP system, where both Hhfac and O₂ sources were directly ionized. Fig. 6 presents the thickness evolution of the HfO₂ film as a function of ALE cycles under repeated exposures to Hhfac gas/O₂ plasma and Hhfac plasma/O₂ plasma for up to 50 cycles at 100 °C. Notably, a consistent thickness reduction with an EPC of 1.49 Å/cycle was observed even at 100 °C, demonstrating a sustained etching effect as the number of ALE cycles increased to 50. This observation clearly indicates that the decomposed adsorption of Hhfac molecules during exposure is essential for effective etching. To reiterate the adsorption mechanism as illustrated in Fig. S7, thus, the gaseous Hhfac molecules are subject to bind to the surface in monodentate, bidentate, and chelate forms without any significant thermal decomposition at low temperatures. During the subsequent O radical pulse, these chemisorbed fluoroketone moieties are not effectively removed through the formation of volatile Hf-fluoroketone complexes, resulting in negligible etching. However, elevating the substrate temperatures or turning on plasma can trigger decomposition of Hhfac ligands, promoting the dissociative adsorption of fluorine-related F_x, CF_x and OCF_x groups. These dissociated species can undergo through the following oxidative destruction with O radicals, leading to the synergistic etching in the various form of volatile products such as Hf-CF, Hf-OCF₂, and Hf-CF₃.

Therefore, it is worthy to note that the etching behavior of high-k oxides with 4+ oxidation states such as HfO₂ is fundamentally governed by the temperature-dependent adsorption modes of the Hhfac precursor. Specifically, while chemisorption alone is insufficient for etching, dissociative adsorption plays a crucial role in facilitating the formation of volatile etch products, overcoming the inherent difficulty in volatilizing high-valency metal oxides. By systematically investigating this mechanism through a combination of experimental results and both *ex-situ* and *in-situ* spectroscopic analyses, we have established an ALE strategy that enables the effective etching of materials with 4+ oxidation states, a challenge that has remained unresolved in conventional Hacac- or Hhfac-based processes. This advancement not only provides critical insights into the etching chemistry of high-k materials but also lays the groundwork for integrating ALE into next-generation semiconductor manufacturing. Given the increasing complexity of future device architectures, our findings offer a promising solution for atomic-level control in advanced patterning and material engineering.

4. Conclusions

We have successfully developed an ALE method effective for various high-k dielectrics, including HfO₂, ZrO₂, Al₂O₃, and Y₂O₃ films, using Hhfac in sequential combination with the Hhfac molecules and O radicals. The ALE process exhibited temperature-dependent etching behaviors, yielding the EPC values of 0.59 Å/cycle, 0.84 Å/cycle, 0.69 Å/cycle, and 0.05 Å/cycle for HfO₂, ZrO₂, Al₂O₃, and Y₂O₃, respectively, within the optimal ALE bias power window at 300 °C. In contrast, negligible etching was observed for Si, SiO₂, and SiN films under the same conditions. Surface roughness measurements confirmed a significant improvement in film smoothness after etching, demonstrating the capability of ALE for precise, atomic-scale material removal. Through

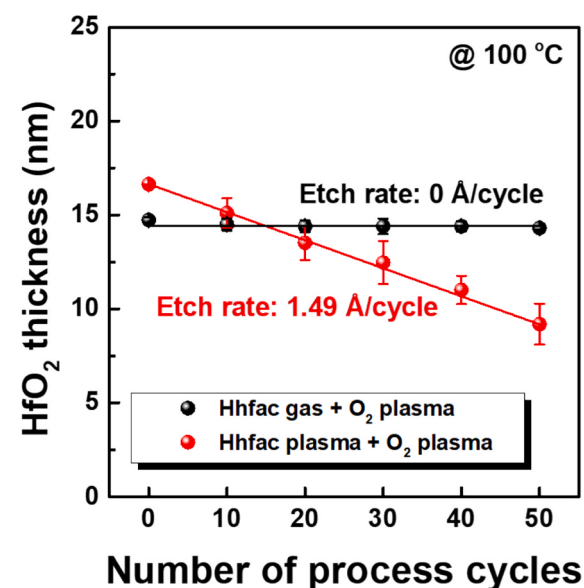


Fig. 6. Thickness variation of the HfO₂ film as a function of ALE cycles under repeated injections of Hhfac gas/O₂ plasma and Hhfac plasma/O₂ plasma at a substrate temperature of 100 °C. CCP discharges at a frequency of 13.56 MHz are applied via an RF power generator.

various spectroscopic analyses, we identified that thermal dissociation during Hhfac adsorption plays a key role in enabling an efficient ALE process. At lower temperatures, chemisorption is the dominant adsorption mode, while at elevated temperatures, it transitions to dissociative adsorption. Subsequently, oxygen radicals interact with fluoro-ether fragments generated from the dissociative adsorption of Hhfac molecules, facilitating the release of volatile Hf-fluoroketone complexes. The current ALE work demonstrates significant efficacy, particularly in the precise etching of high-k dielectrics with high oxidation states, overcoming challenges typically associated with Hacac- or Hhfac-based processes. These findings provide a comprehensive understanding of the chemical and mechanistic aspects of ALE, laying a solid foundation for future advancements in nanoscale device fabrication and semiconductor integration.

CRediT authorship contribution statement

Jeongbin Lee: Writing – original draft, Validation, Methodology, Investigation, Formal analysis, Data curation. **Jieun Oh:** Writing – original draft, Validation, Methodology, Investigation, Formal analysis, Data curation. **Jung-Tae Kim:** Validation, Methodology, Formal analysis. **Jiwoo Oh:** Validation, Methodology, Formal analysis. **Jeong-Min Lee:** Validation, Methodology, Formal analysis. **Woo-Hee Kim:** Writing – review & editing, Supervision, Project administration, Methodology, Funding acquisition, Conceptualization.

Declaration of competing interest

The authors declare that they have no known competing financial interests or personal relationships that could have appeared to influence the work reported in this paper.

Acknowledgments

This work was supported by the National Research Foundation of Korea (NRF) grant funded by the Korea government (MSIT) (2022R1A2C2009941, RS-2023-00258557). This work was supported by the Technology Innovation Program (00233263) funded by the Ministry of Trade, Industry & Energy (MOTIE, Korea). This work was

also financially supported by the Ministry of Trade, Industry and Energy (MOTIE, Korea) and Korea Institute for Advancement of Technology (KIAT) through the International Cooperative R&D program (Task No. P0028466).

Appendix A. Supplementary data

Supplementary data to this article can be found online at <https://doi.org/10.1016/j.cej.2025.163280>.

Data availability

Data will be made available on request.

References

- [1] A.J.M. Mackus, J.R. Schneider, C. Maclsaac, J.G. Baker, S.F. Bent, Synthesis of Doped, Ternary, and Quaternary Materials by Atomic Layer Deposition: A Review, *Chem. Mater.* 31 (4) (2019) 1142–1183.
- [2] A.J.M. Mackus, A.A. Bol, W.M.M. Kessels, The use of atomic layer deposition in advanced nanopatterning, *Nanoscale* 6 (19) (2014) 10941–10960.
- [3] J.-H. Ahn, S.-H. Kwon, Sub-0.5 nm Equivalent Oxide Thickness Scaling for Si-Doped $Zr_{1-x}Hf_xO_2$ Thin Film without Using Noble Metal Electrode, *ACS Appl. Mater. Interfaces*, 7 (28) (2015) 15587–15592.
- [4] V.H. Nguyen, A. Sekkat, C. Jimenez, D. Munoz, D. Bellet, D. Munoz-Rojas, Impact of precursor exposure on process efficiency and film properties in spatial atomic layer deposition, *Chem. Eng. J.* 403 (2021) 126234.
- [5] S. Van Elshocht, C. Adelmann, P. Lehnens, S. De Gendt, Equivalent Oxide Thickness Reduction for High-k Gate Stacks by Optimized Rare-Earth Silicate Reactions, *Electrochem. Solid State Lett.* 12 (5) (2009) G17.
- [6] N. Inoue, J. Sano, T. Kikuchi, Y. Okamoto, K. Nakazawa, T. Miyamoto, Y. Iino, T. Yoshimori, M. Yamage, S. Jimbo, Atomic layer etching process application to TaO hard-mask etching for next-generation EUV (Extreme-Ultraviolet) photomask fabrication, *Photomask Technology* 2024 (13216) (2024) 54–58.
- [7] H. Mertens, R. Ritzenthaler, Y. Oniki, P.P. Gowda, G. Mannaert, F. Sebaai, A. Hikavyy, E. Rosseel, E. Dupuy, A. Peter, K. Vandersmissen, D. Radisic, B. Briggs, D. Batuk, J. Geypen, G. Martinez-Alanis, F. Seidel, O. Richard, B.T. Chan, J. Mitard, E. D. Litta, N. Horiguchi, Forksheet FETs with Bottom Dielectric Isolation, Self-Aligned Gate Cut, and Isolation between Adjacent Source-Drain Structures, 2022 International Electron Devices Meeting (IEDM), 2022, 23.1.1-23.1.4.
- [8] M.F.J. Vos, S.N. Chopra, M.A. Verheijen, J.G. Ekerdt, S. Agarwal, W.M.M. Kessels, A.J.M. Mackus, Area-Selective Deposition of Ruthenium by Combining Atomic Layer Deposition and Selective Etching, *Chem. Mater.* 31 (11) (2019) 3878–3882.
- [9] H.-B. Kim, J.-M. Lee, D. Sung, J.-H. Ahn, W.-H. Kim, Highly area-selective atomic layer deposition of device-quality $Hf_{1-x}Zr_xO_2$ thin films through catalytic local activation, *Chem. Eng. J.* 488 (2024) 150760.
- [10] I.L. Berry, K.J. Kanarik, T. Lill, S. Tan, V. Vahedi, R.A. Gottscho, Applying sputtering theory to directional atomic layer etching, *J. Vac. Sci. Technol. A* 36 (1) (2017).
- [11] J.B. Park, W.S. Lim, B.J. Park, I.H. Park, Y.W. Kim, G.Y. Yeom, Atomic layer etching of ultra-thin HfO_2 film for gate oxide in MOSFET devices, *J. Phys. d: Appl. Phys.* 42 (5) (2009) 055202.
- [12] K.M. Lutker-Lee, Y.-T. Lu, Q. Lou, J. Kaminsky, Y. Kikuchi, A. Raley, Low-k dielectric etch challenges at the 7 nm logic node and beyond: Continuous-wave versus quasiatomic layer plasma etching performance review, *J. Vac. Sci. Technol. A* 37 (1) (2018).
- [13] X. Sang, J.P. Chang, Physical and chemical effects in directional atomic layer etching, *J. Phys. d: Appl. Phys.* 53 (18) (2020) 183001.
- [14] M. Konh, C. He, X. Lin, X. Guo, V. Pallem, R.L. Opila, A.V. Teplyakov, Z. Wang, B. Yuan, Molecular mechanisms of atomic layer etching of cobalt with sequential exposure to molecular chlorine and diketones, *J. Vac. Sci. Technol. A* 37 (2) (2019).
- [15] S. Fujisaki, Y. Yamaguchi, H. Kobayashi, K. Shinoda, M. Yamada, H. Hamamura, K. Kawamura, M. Izawa, Thermal-cyclic atomic layer etching of cobalt with smooth etched surface by plasma oxidation and organometallization, *Appl. Phys. Lett.* 121 (12) (2022).
- [16] E. Mohimi, X.I. Chu, B.B. Trinh, S. Babar, G.S. Girolami, J.R. Abelson, Thermal Atomic Layer Etching of Copper by Sequential Steps Involving Oxidation and Exposure to Hexafluoroacetyleacetone, *ECS. J. Solid State Sci. Technol.* 7 (9) (2018) P491.
- [17] A. Mameli, M.A. Verheijen, A.J.M. Mackus, W.M.M. Kessels, F. Roozeboom, Isotropic Atomic Layer Etching of ZnO Using Acetylacetone and O_2 Plasma, *ACS Appl. Mater. Interfaces*, 10 (44) (2018) 38588–38595.
- [18] J.L. Partridge, A.I. Abdulagatov, V. Sharma, J.A. Murdzek, A. Cavanagh, S. M. George, Thermal atomic layer etching of CoO using acetylacetone and ozone: Evidence for changes in oxidation state and crystal structure during sequential exposures, *Appl. Surf. Sci.* 638 (2023) 157923.
- [19] S.R. Droses, T.T. Kodas, M.J. Hampden-Smith, Etching of ZnO Films with Hexafluoroacetyleacetone, *Adv. Mater.* 10 (14) (1998) 1129–1133.
- [20] S. Yun, F. Ou, H. Wang, M. Tom, G. Orkoulas, P. Christofides, Atomistic-Mesoscopic Modeling of Area-Selective Thermal Atomic Layer Deposition, *Chem. Eng. Res. Des.* 188 (2022) 271–286.
- [21] S. Yun, M. Tom, J. Luo, G. Orkoulas, P. Christofides, Microscopic and Data-Driven Modeling of Thermal Atomic Layer Etching of Aluminum Oxide Thin Films, *Chem. Eng. Res. Des.* 177 (2022) 96–107.
- [22] M. Kim, J. Kim, S. Kwon, S.H. Lee, H. Eom, B. Shong, Theoretical Design Strategies for Area-Selective Atomic Layer Deposition, *Chem. Mater.* 36 (11) (2024) 5313–5324.
- [23] N.B. Morozova, K.V. Zherikova, I.A. Bairina, S.V. Sysoev, P.P. Semyannikov, L. V. Yakovkina, T.P. Smirnova, N.V. Gelfond, I.K. Igumenov, G. Carta, G. Rossetto, Volatile hafnium(IV) compounds with beta-diketonate and cyclopentadienyl derivatives, *J. Phys. Chem. Solids* 69 (2) (2008) 673–679.
- [24] K.V. Zherikova, N.B. Morozova, N.V. Kurat'eva, I.A. Bairina, P.A. Stabnikov, I. K. Igumenov, X-ray structural study of fluorinated β -diketonate complexes of zirconium(IV), *J. Struct. Chem.* 48 (3) (2007) 513–522.
- [25] V.G. Dashevskii, A.P. Baranov, M.I. Kabachnik, Steric Aspects of the Formation of Metal Chelate Complexes, *Russ. Chem. Rev.* 52 (2) (1983) 152.
- [26] O. Maida, K.-I. Fukayama, M. Takahashi, H. Kobayashi, Y.-B. Kim, H.-C. Kim, D.-K. Choi, Interface states for HfO_2/Si structure observed by x-ray photoelectron spectroscopy measurements under bias, *Appl. Phys. Lett.* 89 (12) (2006).
- [27] H.Y. Zhang, C. Ye, C.G. Jin, M.Z. Wu, Y.Y. Wang, Z. Zhang, T.Y. Huang, Y. Yang, H. J. He, L.J. Zhuge, X.M. Wu, Electrical properties improvement of high-k HfO_2 films by combination of C_4F_8 dual-frequency capacitively coupled plasmas treatment with thermal annealing, *Appl. Surf. Sci.* 311 (2014) 117–123.
- [28] J. Shang, G. Liu, H. Yang, X. Zhu, X. Chen, H. Tan, B. Hu, L. Pan, W. Xue, R.-W. Li, Thermally Stable Transparent Resistive Random Access Memory based on All-Oxide Heterostructures, *Adv. Funct. Mater.* 24 (15) (2014) 2171–2179.
- [29] C.E. Moffitt, Q.S. Yu, C.M. Reddy, D.M. Wieliczka, H.K. Yasuda, XPS Analysis of the Aging of Thin, Adhesion Promoting, Fluorocarbon Treatments of DC Plasma Polymers, *Plasma Polym.* 6 (4) (2001) 193–209.
- [30] A. Gharachorlou, M.D. Detwiler, A.V. Nartova, Y. Lei, J. Lu, J.W. Elam, W. N. Delgass, F.H. Ribeiro, D.Y. Zemlyanov, Palladium Nanoparticle Formation on $TiO_2(110)$ by Thermal Decomposition of Palladium(II) Hexafluoroacetyleacetone, *ACS Appl. Mater. Interfaces*, 6 (16) (2014) 14702–14711.
- [31] W.-H. Kim, K. Shin, B. Shong, L. Godet, S.F. Bent, Atomic Layer Deposition of Pt on the Surface Deactivated by Fluorocarbon Implantation: Investigation of the Growth Mechanism, *Chem. Mater.* 32 (22) (2020) 9696–9703.
- [32] G. Nansé, E. Papirer, P. Fioux, F. Moguet, A. Tressaud, Fluorination of carbon blacks: An x-ray photoelectron spectroscopy study: I. A literature review of XPS studies of fluorinated carbons. XPS investigation of some reference compounds, *Carbon* 35 (2) (1997) 175–194.
- [33] H.J. Ahn, J.B. Kim, B.H. Hwang, H.K. Baik, J.S. Park, D. Kang, Structural and chemical characterization of fluorinated amorphous carbon films (a-C:F) as a liquid crystal alignment layer, *Diam. Relat. Mater.* 17 (12) (2008) 2019–2024.
- [34] H.T. Sahin, RF- CF_4 Plasma Treatment of Tetrafluoroethane Pre-deposited Paper, Part 1: Hypotheses on Surface Reactions, *J. Wood Chem. Technol.* 40 (2) (2020) 91–104.
- [35] W. Zhengyu, Y. Yintang, W. Jiayou, Structural, thermal and electrical properties of plasma deposited a-C:F films, in: Polytronic 2005-5th International Conference on Polymers and Adhesives in Microelectronics and Photonics, 2005, pp. 210–214.
- [36] K.-Y. Lin, C. Li, S. Engelmann, R.L. Bruce, E.A. Joseph, D. Metzler, G.S. Oehrlein, Selective atomic layer etching of HfO_2 over silicon by precursor and substrate-dependent selective deposition, *J. Vac. Sci. Technol. A* 38 (3) (2020).
- [37] J.-W. Lee, S.-P. Jeong, N.-H. You, S.-Y. Moon, Tunable Synthesis of Predominant Semi-Ioniz and Covalent Fluorine Bonding States on a Graphene Surface, *Nanomater.* 11 (4) (2021) 942.
- [38] G.I. Semushkina, Y.V. Fedoseeva, A.A. Makarova, D.A. Smirnov, I.P. Asanov, D. V. Pinakov, G.N. Chekhova, A.V. Okotrub, L.G. Bulusheva, Photolysis of Fluorinated Graphites with Embedded Acetonitrile Using a White-Beam Synchrotron Radiation, *Nanomater.* 12 (2) (2022) 231.
- [39] H. Kung, A. Teplyakov, Selectivity and mechanism of thermal decomposition of β -diketones on ZnO powder, *J. Catal.* 330 (2015) 145–153.
- [40] S. Engmann, B. Ómarsson, M. Lacko, M. Stano, S. Matejčík, O. Ingólfsson, Dissociative electron attachment to hexafluoroacetyleacetone and its bidentate metal complexes $M(hfac)_2$; $M = Cu, Pd$, *J. Chem. Phys.* 138 (23) (2013).
- [41] A.H. Basher, I. Hamada, S. Hamaguchi, Self-Limiting Processes in Thermal Atomic Layer Etching of Nickel by Hexafluoroacetyleacetone, *Jpn. J. Appl. Phys.* 59 (9) (2020) 090905.
- [42] N.R. Rueger, J.J. Beulens, M. Schaeckens, M.F. Doemling, J.M. Mirza, T.E.F. M. Standaert, G.S. Oehrlein, Role of steady state fluorocarbon films in the etching of silicon dioxide using CHF_3 in an inductively coupled plasma reactor, *J. Vac. Sci. Technol. A* 15 (4) (1997) 1881–1889.